Tribol Lett (2010) 39:295–309
DOI 10.1007/s11249-010-9662-9

ORIGINAL PAPER

Mechanical Response and Energy-Dissipation Processes in Oligothiophene Monolayers Studied with First-Principles Simulations

Wojciech Kamiński · Rubén Pérez

Received: 6 February 2010 / Accepted: 10 July 2010 / Published online: 28 July 2010

Abstract We present an extensive first-principles study of the interaction between a silicon oxide nanoasperity and a sexithiophene monolayer in order to investigate the individual molecular processes responsible for the energy dissipation during atomic force microscope (AFM) operation. Our approach includes not only ground-state calculations of the tip–sample interaction, but an extensive set of molecular dynamics simulations at room temperature to include the folding deformation modes that are necessary to describe properly the mechanical response on the molecular layer. With this large computational effort, we have characterized the complex configuration space of the combined tip–sample system in a function of the distance, position and orientation of the tip. We identify surface adhesion as the relevant short-range dissipation mechanism. The system is trapped, due to the presence of energy barriers that cannot be overcome even with the available thermal energy, in different bonding configurations corresponding to local energy minima during the approach and retraction of the tip. These energy barriers are responsible for breaking the adiabaticity and thus lead to force hysteresis and energy dissipation. The quantitative agreement between our calculations and experimental results for the mechanical strength and the dissipated energy supports the use of combined theoretical–experimental dynamic AFM studies in order to gain a fundamental understanding of the microscopic mechanisms involved in energy dissipation.

W. Kamiński
Institute of Experimental Physics, University of Wrocław, plac Maksa Borna 9, 50-204 Wrocław, Poland

W. Kamiński · R. Pérez (✉)
Departamento de Física Teórica de la Materia Condensada, Universidad Autónoma de Madrid, 28049 Madrid, Spain
e-mail: ruben.perez@uam.es

Keywords AFM · Adhesion · Ab initio simulations · Molecular dynamics simulations · Contact mechanics · Oligothiophenes

1 Introduction

Friction and adhesion are ultimately originated by the interaction of multiple nanoasperities between two bodies in contact [1]. Although significant advances in the description and control of friction have been achieved in the last few years, the physical mechanisms of energy dissipation during friction remain controversial and are still poorly understood. The atomic force microscope (AFM), where a sharp tip—a single nanoasperity—interacts with a surface, provides a model system for the fundamental research of such complex phenomena. Different AFM-based experimental techniques have been developed in order to access the mechanical and friction properties of single contacts. While most of the classical studies are based on the friction force microscope (FFM) [2], dynamical AFM methods—that provide access to well-defined contact geometries involving just few atoms—are emerging as unique tools to measure energy dissipation and to identify the underlying microscopic processes. At variance with the FFM, where the tip and sample remain in contact under a large repulsive force during scan and the force is determined directly from the cantilever deflection, in the dynamic AFM operation, the changes in the amplitude, the resonance frequency and the phase-shift of the oscillation link the dynamics of a vibrating tip to the tip–surface interactions. Our goal in this contribution is to show how experiments based on dynamic AFM and theoretical simulations can be combined in order to provide a

framework for the quantitative study and characterization of the dissipation processes at the nanometer and atomic scale. Presently, two major dynamic AFM modes, amplitude modulation (AM-AFM or tapping mode) and frequency modulation (FM-AFM) have being developed to measure the topography of a sample surface [3]. AM-AFM exploits the reduction of the oscillation amplitude by the tip–sample interaction. This amplitude change is used—in the same way as the tunnelling current variation with distance in the scanning tunnelling microscope (STM)—as a feedback parameter to produce topographical images. AM-AFM achieves nanometer-scale spatial resolution in soft materials (including biological samples) [3–5]. In FM-AFM (commonly known as non-contact AFM, NC-AFM), the focus is set on how the resonance frequency of the cantilever is affected by the tip–sample interaction while keeping the cantilever oscillating always with the same amplitude. The control over the interaction of the tip outermost atom with the surface provides true atomic resolution in metal, semiconductor and insulating surfaces [6–9]. While traditionally performed in ultra-high vacuum, recent developments have extended the FM-AFM high-resolution capabilities to technologically relevant environments, including liquids [10, 11].

Apart from topography, both major dynamical AFM methods provide access to information about energy-dissipation processes during tip–sample contact. In AM-AFM, it was soon realized that the variation of the phase-shift—the phase lag between the external excitation of the vibrating probe and its response to the tip–surface interactions—gives rise to a powerful source of spatial contrast. This method is known as phase-imaging force microscopy [12]. Notice that dissipation at the nanoscale can be accomplished in a wearless regime that it is compatible with high-resolution imaging. Thus, the measurement of the changes in amplitude and phase confers AM-AFM the ability to map simultaneously the shape and the compositional variations of heterogeneous materials.

The phase-shift is, in principle, related to the local energy dissipation on the surface [13–15]. The theory of amplitude modulation AFM at high-quality factors is based on the use of a point-mass model to calculate the properties and interactions of a vibrating tip in the proximity of a surface, including the sample deformation and adhesion properties through continuum mechanics modelling [16, 17]. This approach has demonstrated great quantitative accuracy in the description of AM-AFM experiments [18–20]. Considering this success, it is surprising the lack of studies devoted to link the observed contrast in phase-imaging with atomic and molecular energy-dissipating processes. It is only very recently, that phase-imaging has been applied to identify nanoscale dissipation processes [21]. This first step has not been followed by any attempt to understand from a fundamental perspective the atomistic and molecular mechanisms responsible for these dissipative processes, in particular for the surface adhesion hysteresis.

The true-atomic-resolution of FM-AFM provides experimental access to study the most basic and *well defined* case one could think about: the friction and adhesion originated in a single atomic contact [22]. Two different signals are simultaneously recorded in FM-AFM [3, 23]: the frequency shift that renders the topography, and the so-called dissipation (or damping) signal: the additional amount of energy required to keep the oscillation amplitude constant, compensating for the energy lost in the cantilever due to the non-conservative tip–sample interactions. The dissipation images show also true atomic resolution and thus provide a tool to study dissipation at the atomic scale. While a general consensus exist in the interpretation of the topography images, the connection between the dissipation images and some physical energy-dissipation processes have been very controversial [24–29]. This is related to the fact that, even for the case of a single atomic contact, reliable quantitative studies require, the characterization of the tip-apex termination [30], quite a complicated task commonly avoided.

Recently, an FM-AFM study on a well-characterized semiconductor surface (Ge(111)-c(2 $\times$ 8)) [31], where it was possible to switch between two different topographic and dissipation patterns on the same surface by a gentle contact of the tip and the surface, has unambiguously identified a dissipation channel due to single atomic contact adhesion and the associated atomic processes. Combining force and dissipation spectroscopy measurements (obtained from the distance variation of the corresponding signal) with large-scale ab initio density functional theory (DFT) calculations (involving more than 300 atoms in the unit cell), it was possible to identify the detailed geometry and composition of the tip-apex and its influence on the energy dissipation [31]. This dissipation channel is characterized by two different solutions in the short-range force upon the tip-apex approach and retraction with a notable hysteresis between them. At atomic level, this mainly manifests in the breaking and remaking of a single bond between the probed adatom and the surface atom induced by a stronger adhesion with the tip-apex upon the retraction. This dissipation mechanism is common to other semiconductor surfaces and interfaces (see the supplementary information in reference [32]).

Motivated by the successful combination of theory and FM-AFM experiments for the understanding of adhesion hysteresis at the atomic scale described above, in this contribution, we have combined phase-imaging experimental measurements of the energy transferred by a silicon dioxide tip into a region of sexithiophene (T6) molecules,

with continuum modelling and first-principles calculations for the tip–molecular layer interaction in order to identify the molecular processes responsible for energy dissipation. T6, a widely studied organic material, is a linear molecule formed by six thienyl rings (see Fig. 1) that forms densely packed molecular layers with an herringbone arrangement [33, 34]. T6 is both interesting for technological applications—it is considered one of the best performing semiconductors in field-effect transistors based on organic thin films—and from a basic perspective, as it offers the opportunity to investigate the interplay between intramolecular, intermolecular and lattice dissipation channels.

The experimental details and a brief description of the theoretical aspects of this combined study has been already presented in reference [35]. Here, we focus on the theoretical challenge posed by the first-principles simulations of T6. In order to describe properly the mechanical response of this organic material at room temperature (RT), it is necessary to include collective deformation modes (folding modes, see Sect. 4.2) that are not active in the usual $T = 0$ K calculations for the tip–sample interaction. We achieve this goal performing a set of large-scale first-principles molecular dynamics simulations at $T = 300$ K, involving almost 400 atoms, one for each tip height and position over the surface considered. In this way, we can determine realistic tip–sample force curves for the approach and retraction parts of the oscillation cycle and discuss the molecular processes responsible for energy dissipation associated with adhesion during the tip–molecular layer mechanical contact.

The rest of the article is organized as follows. In Sect. 2, we summarize how the experimental short-range contribution to the energy dissipation (1.4 eV/cycle) during the mechanical contact can be extracted from dissipated energy versus oscillation amplitude curves taken in both the attractive and repulsive regimes with the aid of contact mechanics modelling. Section 3 discusses the details of the first-principles simulations, the atomistic models for the tip and the sample, as well as the mechanical characterization of both the T6 molecule and the monolayer. The core of the paper is presented in Sect. 4, where we discuss the limitations of first-principles calculations at $T = 0$ K for a silicon oxide nanoasperity interacting with a T6 monolayer, and how we overcome this problem with a set of molecular dynamics simulations. These reliable approach/retraction force curves match the sample mechanical response and the energy dissipated per molecular chain in the experiments ($\sim$0.15 eV/cycle) for the same indentation depth and contact size determined with the continuum modelling. Then, we show how these simulations identify adhesion hysteresis as the dominant source of dissipation and shed light on the molecular mechanisms involved (Sect. 5). Our study shows that the hysteresis in the short-range force is related to the rich configuration space of the sample: the system is trapped, due to the presence of energy barriers, in different bonding configurations corresponding to local energy minima during the approach and retraction of the tip. Section 6 summarizes our main results and discusses the possible use of dynamic AFM to understand friction at the atomic scale.

2 Extracting the Short-Range Contribution to Dissipation: Phase-Imaging Measurements and Contact Mechanics Modelling

The energy dissipated per cycle (E_{dis}) due to the tip–sample interaction can be extracted from experimental measurements of the oscillation amplitude, A, and the phase-shift ϕ between the external excitation and the tip response through the equation [36]:

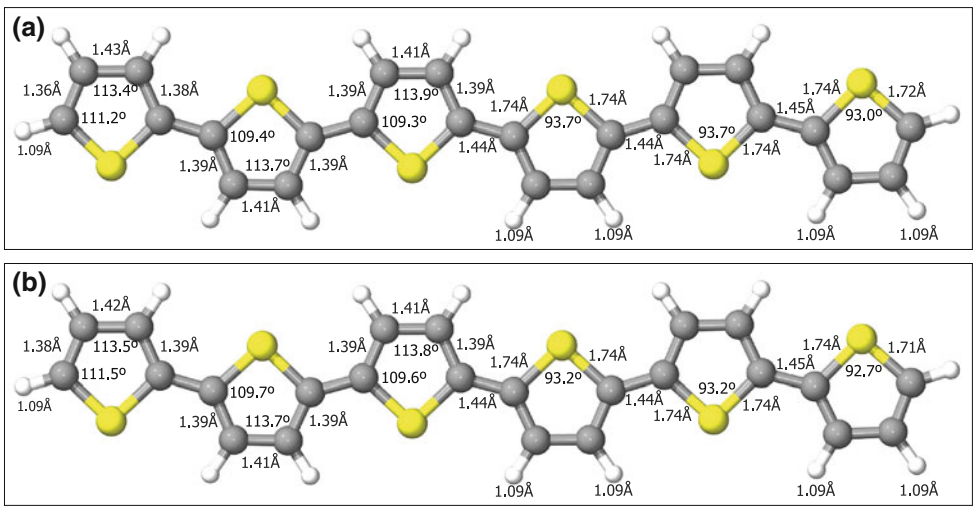

Fig. 1 Schematic illustration of the T6 molecule indicating the main structural parameters extracted from the optimization of the molecular geometry with first-principles simulations based on **a** FIREBALL and **b** VASP codes. Color code for the atoms: hydrogen (*white*), sulphur (*yellow*), and carbon (*grey*). (Color figure online)

$$E_{\mathrm{dis}} = \frac{\pi k A}{Q}\left(A_0 \sin\phi - \frac{A\omega}{\omega_0}\right), \quad (1)$$

where Q and k are the quality factor and force constant of the cantilever; A_0 is the amplitude very far from the surface; ω_0 and ω are, respectively, the first resonance and excitation frequencies. As the possible dissipation mechanisms—including surface adhesion, long-range interfacial interactions and viscoelasticity—have a significantly different variation with distance, the variation of the energy dissipated as a function of the operating conditions can help to single out its contribution. This goal can be achieved through the dynamic-dissipation curves [36]: a representation of the average energy transferred by tip to the sample surface as a function of oscillation amplitude while the tip approaches the surface.

Figure 2a shows the experimental dynamic-dissipation curves measured on top of T6 islands for both the attractive and the repulsive regime. Details concerning the sample preparation, the AFM operation conditions and the individual experimental steps to measures those curves can be found in reference [35]. The shape of these curves singles out the contribution of the different dissipation processes (see reference [21] and the discussion below). The symmetric shape of the lower curve (red) corresponds to the presence of long-range interfacial interactions, while the almost-flat upper curve (green) reveals the mechanical contact between tip and sample and the opening of another channel, associated to surface adhesion, that can be described in terms of surface energy hysteresis [21]. One may naively think that the short-range contribution to dissipation can be determined just substracting the two curves in Fig. 2a. The complex dynamics of the cantilever, that explores a different distance range in the attractive and repulsive branches [3], prevents this simple procedure. The basis for extracting the short-range contribution to dissipation from the experimental data using continuum mechanics modelling is described below.

The dynamic response of the cantilever–tip ensemble driven by an external and sinusoidal signal in the proximity of a surface is usually simulated using the following second-order differential equation:

$$m\frac{\mathrm{d}^2 z}{\mathrm{d}t^2} = -kz - \frac{m\omega_0}{Q}\frac{\mathrm{d}z}{\mathrm{d}t} + F_0\cos(\omega t) + F_{\mathrm{ts}}. \quad (2)$$

In this approach, we assume a point-mass model for the cantilever–tip ensemble that has been shown to reproduce AM-AFM experiments where the contribution of higher cantilever eigenmodes can be neglected [37, 38]. The dominant contributions considered in this equation of motion are the cantilever elastic response, the hydrodynamic damping with the medium, the excitation force, and the tip–sample interaction. The Q factor used here is independent of tip–sample separation, neglecting changes in the hydrodynamic damping of the cantilever during its motion.

The critical issue is the description of the tip–sample interaction. The tip–sample geometry is simulated by a sphere (tip) and a flat (sample). The tip–sample interaction contains both attractive and repulsive forces. Long-range attractive forces are derived from the nonretarded van der Waals (vdW) interaction. For a sphere–flat geometry, the vdW force depends quadratically on the tip–sample distance:

$$F_{\mathrm{vdW}} = -\frac{HR}{6d^2} = -\frac{\alpha}{d^2}, \quad (3)$$

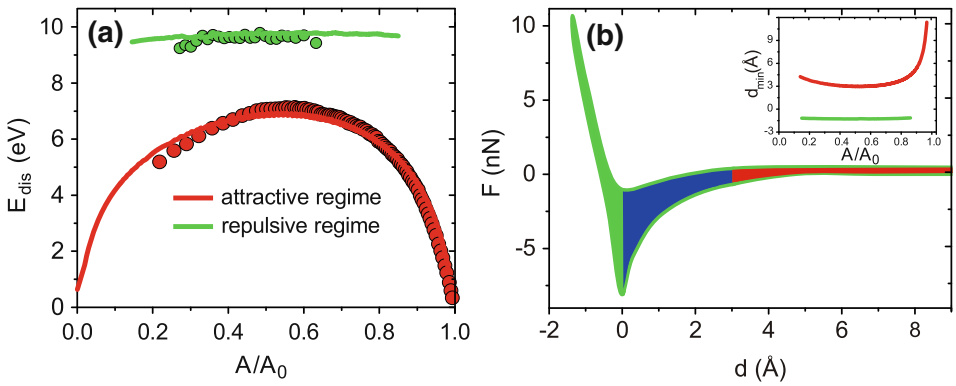

Fig. 2 **a** Energy dissipation dependence on the normalized oscillation amplitude for the attractive (*red*) and repulsive (*green*) regimes. The experimental curves (*circles*) are faithfully reproduced by a point-mass simulation (*solid lines*) that uses DMT contact mechanics and van der Waals forces. **b** Force–distance curve that reproduces the experiments is shown in **a**. The *thick green line* shows the force during approach (*upper part*) and retraction (*lower part*) in the repulsive regime. The *blue region* remains experimentally unexplored in the attractive regime because the minimum tip–sample distance is about 3 Å, while the tip indents up to −1.4 Å in the repulsive regime (see *inset*) (adapted from reference [35]). (Color figure online)

where H is the Hamaker constant and R the tip radius.

The sample deformation and its associated stress is calculated by the Derjaguin–Muller–Toporov (DMT) model [17]:

$$F_{\mathrm{DMT}} = Y^{*}R^{1/2}\delta^{3/2} - 4\pi R\gamma, \tag{4}$$

where δ is the deformation (indentation), Y^{*} is the effective elastic modulus of the interface, R is the tip radius, and γ is the surface energy, that introduces adhesion effects into the model.

In order to reproduce the dynamic-dissipation curves measured in the experiment, we generalize the conservative forces described above in order to include non-conservative interactions into the model [21]. Long-range dissipative interfacial forces, i.e., interactions that do not imply the mechanical contact between probe and surface (noncontact) are calculated by using a time-dependent interaction with the same distance dependence of the vdW force but where the strength depends on whether the probe approaches (α_{a}) or retracts away (α_{r}) from the surface. The energy dissipated by adhesion hysteresis is simulated assuming in the DMT force different values for the surface energy during approach (γ_{a}) and retraction (γ_{r}). Within this model, the energy dissipated per cycle is given by the sum of the following contributions:

$$E_{\mathrm{dis}}^{\mathrm{adhesion}} = \oint F_{\mathrm{DMT}}\mathrm{d}z = 4\pi R\delta(\gamma_{\mathrm{r}} - \gamma_{\mathrm{a}}), \tag{5}$$

and

$$E_{dis}^{\mathrm{vdW}} = \oint \frac{\alpha(t)}{d^{2}}\mathrm{d}z = (\alpha_{a} - \alpha_{r})\left(\frac{1}{d_{1}} - \frac{1}{d_{2}}\right), \tag{6}$$

where d_1 and d_2 are, respectively, the closest and the farthest tip–surface separation during a cycle.

The experimental dynamic-dissipation curves for T6 for both the attractive and repulsive regime (red and green circles in Fig. 2a, respectively) can be faithfully reproduced by dynamical simulations (red and green solid lines) in considering both long-range dissipative interactions and surface energy hysteresis in the tip–surface interaction defined by the following set of parameters: $R = 7$ nm, $Y^{*} = 60$ GPa, $\alpha_{\mathrm{a}} = 7 \times 10^{-28}$ Jm and $\gamma_{\mathrm{a}} = 50$ mJ/m^2; $\alpha_{\mathrm{r}} = 3\alpha_{\mathrm{a}}$ and $\gamma_{\mathrm{r}} = 57$ mJ/m^2. Notice for reference that similar curves on the silicon substrate require an effective bulk modulus $Y^{*} = 170$ GPa. These simulations were performed by solving numerically the equation of motion (Eq. 2) with a fourth order Runge–Kutta algorithm. Figure 2b shows the theoretical (continuum model) force versus distance curve that describe the experimental dissipation curves. The hysteresis observed between the force during loading and uploading of the tip gives rise to dissipation. The dissipated energy grows in the repulsive regime due to the large contribution associated to adhesion, that is modelled through the differences in surface energy.

This analysis shows that dissipation at the nanoscale can be described in terms of force hysteresis provided that we include both contributions coming from long-range interactions and from short-range atomic and molecular interactions [17, 21]. Compositional contrast in phase-imaging AFM could be obtained in both regimes, although the contrast achieved in the repulsive regime is usually sharper. Furthermore, the contrast in the attractive regime could have a residual contribution from capillary forces [39]. Those contributions are not directly related to material properties of the sample surface. For this reason, we focus on the contact regime to perform a quantitative comparison between experiments and first-principle calculations.

The theoretical curves show that the measurements performed in the repulsive regime contain contributions from both short and long-range dissipation effects. One can naively consider that just a direct substration of the energy dissipated in the repulsive and attractive regimes is enough to obtain the short-range contribution. However, this is not the case because a certain range of tip–sample distances is not accessible to the system due to mechanical stability considerations in AM-AFM [3]. As the minimum tip–surface distance in the attractive regime is about 3 Å (see the inset in Fig. 2b), the attractive regime gives only a partial information about the long-range dissipative processes included in the measurements in the repulsive regime (forces for approach and retraction correspond to the thick green lines in Fig. 2b). The blue region in Fig. 2 remains unexplored in the attractive regime. However, the excellent agreement obtained between point-mass simulations and experiments (see Fig. 2a) allows us to determine the energy dissipated in the blue area. Thus, to determine the energy dissipated exclusively through short-range interaction forces (the green region), we subtract from the energy measured in the repulsive regime the energy dissipated through long-range forces (red part) and the energy dissipated corresponding to the blue region (see Fig. 2b). This analysis provides a short-range contribution for T6 of 1.4 eV.

Apart from the long-range and adhesion contributions discussed above, in some cases it is necessary to include viscoelastic effects taken place during mechanical contact in order to account for the dissipation measured in the experiments. Dynamic-dissipation curves associated with these kind of dissipative processes have a distinctive shape [21], so, considering experimental results, described in [35], we can rule out that viscoelastic processes have a significant contribution in the T6 case. Under these conditions, the time scales for the short-range dissipation processes (associated with atomic movements that take place in the picosecond scale) and the tip dynamics (the oscillation frequencies are in the 10–100 kHz range) can be

clearly decoupled. This justifies the quasi-static approach considered in the following sections in order to determine the force versus distance curves using first-principles methods.

3 First-Principles Simulations: Modelling of the System and Computational Details

The basic limitation of the theoretical modelling described so far is the continuum description of the molecular contact in terms of elastic moduli and surface energies. First-principles calculations, based on DFT, can provide significant physical insight into the real deformation mechanisms in the sample and the microscopic origin of the force hysteresis associated with adhesion, that has been introduced so far assuming different surface energies for approach and retraction in order to reproduce the experiments.

From this perspective, we have performed an extensive set of first-principles molecular dynamics simulations for the interaction between a silicon oxide tip and a T6 monolayer in order to investigate the individual molecular processes responsible for the energy dissipation. Our goal is to characterize the complex configuration space of the combined tip–sample system as a function of the distance, in order to identify the atomistic mechanisms that are responsible for the system to be trapped in local energy minima during its evolution, leading to the hysteresis in the force. Given the very different time scales for the tip dynamics and the atomic response, we can actually decouple them, and determine the tip–sample force as a function of the distance using a quasi-static approach, as described below. Notice that we do not attempt to simulate how the mechanical energy associated with this hysteretic behaviour, $\oint F \mathrm{d}z$, is actually dissipated into phonons and, finally, into heat. This study would require a very complex simulation of the actual dynamics of the cantilever–tip–sample ensemble, modelled with a very large unit cell, that is a challenge even for simulations based on classical potentials, and definitely well beyond our current capabilities with ab initio methods.

Our single-asperity simulations are still far from the complex experimental multi-asperity contact. In order to bridge this gap, we are going to combine our first-principles calculations with the continuum modelling. Reproducing the experimental mechanical response for a given indentation depth, we can compare then the dissipated energies (see the end of Sect. 4.3) and thus provide a fundamental understanding of the microscopic mechanisms involved in energy dissipation.

3.1 Modelling the Tip and the Sample

The calculations we have to perform are very computationally demanding and some simplifications on the description of the tip and sample are needed in order to keep them feasible.

Regarding the sample, we need to describe the adsorption of the T6 molecules on the silicon oxide-covered substrate. The modelling of the free oxide surface is still the subject of an intense experimental and theoretical effort. Thus, we have modelled the sample assuming a T6 free-standing monolayer with some of the bottom atoms fixed but no substrate for the adsorption. This simplified approach to the problem captures the key ingredients revealed by the experiments for the adsorption on the oxide: T6 molecules are standing up normal to the surface and their bottom part is almost fixed due to the substrate interaction. The elimination of the substrate also makes possible the consideration of larger surface periodicities. In these simulations, we have taken the important parameter, the molecular packing (characterized by the surface unit cell, that differs from that of molecular planes in the crystal due to the interplay between molecule–molecule and substrate–molecule interactions) with lattice vectors determined from detailed X-ray diffraction experiments [40]. For the ultra thin films considered in our work, the

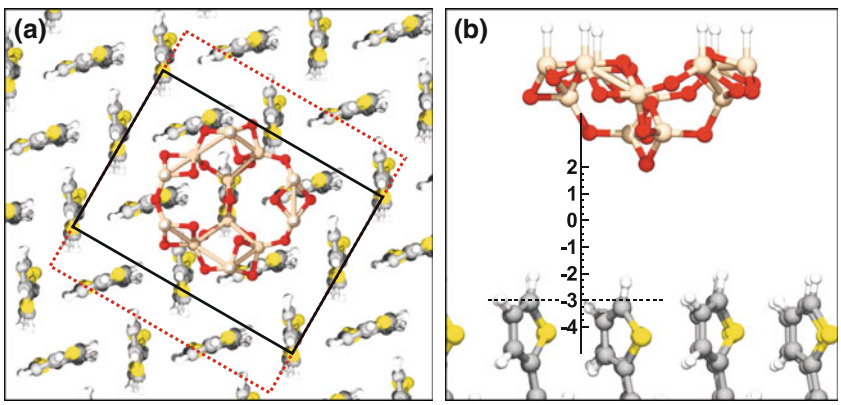

Fig. 3 **a** Top view of the herringbone structure of sexithiophene monolayer and single Si oxide tip stands on top of the molecules. The 4 × 2 (*solid black line*) and 4 × 3 (*dotted red line*) unit cells are marked. **b** Side view of tip–sample interface with a distance reference scale. Color code for the atoms: oxygen (*red*), sulphur (*yellow*), carbon (*grey*), hydrogen (*white*) and silicon (*light salmon*). (Color figure online)

molecules retain the herring-bone arrangement as in the crystal with a slightly contracted in-plane unit cell ($a = 7.70$ Å and $c = 5.52$ Å) with respect to the bulk unit cell ($a = 7.85$ Å and $c = 6.03$ Å [34]). The T6 sample is described by a monolayer of T6 molecules in a 4×2 unit cell, that contains eight molecules in the characteristic herring bone pattern (see Fig. 3a). Test calculations have been performed in a 4×3 unit cell (12 molecules) as discussed below.

Experimental tips are produced by microfabrication techniques on Si wafers and, under the conditions of the experiment, are covered with the Si native oxide. As we are only interested in the short-range interactions, we just need to model the microscopic tip termination. Here, we have resorted to the literature on the structure and energetics of Si oxide clusters. As the tip-apex, we have considered an oxide nanoasperity constructed from a very stable Si oxide cluster [41, 42] (see Fig. 3). This model fulfils all the necessary requirements, while keeping the tip size within the limits of affordable simulations: it provides the high-mechanical stability of the Si oxide and displays at the apex the protruding doubly coordinated oxygen atoms that are expected on the outer layer of the oxide.

In our calculations, we have used a supercell approach (including 391 atoms), where the T6 surface is represented by a 4×2 unit cell (352 atoms), and the AFM tip is modelled with a Si oxide nanoasperity containing 39 atoms. Only the Γ point has been included in the sampling of the Brillouin zone.

3.2 Simulation Method: FIREBALL

Our calculations, performed using the FIREBALL code [43–46], are based on DFT with a local-orbital basis. This code is designed to deal with large-scale simulations and offers a very favorable accuracy-to-efficiency balance provided when the basis set is carefully chosen. The calculations presented in this paper are performed within the local density approximation (LDA) for the exchange-correlation functional [47].

Our work focuses on the understanding of phase-imaging contrast at the molecular level and the identification of the energy dissipation mechanisms that are responsible for this nanometer-scale resolution. The vdW interactions, due to their long-range character, are dominated by the interaction of the macroscopic parts of tip and sample, not by the interaction of the closest atoms. Thus, they do not contribute significantly to the contrast addressed by the experiments discussed in Sect. 2. Our DFT–LDA calculations provide the theoretical framework to determine this short-range chemical force in the relevant near-contact regime and we do not include explicitly the macroscopic vdW. The contribution of the vdW interaction associated with the closest atoms can be certainly neglected in the presence of strong chemical bonding (e.g. covalent, metallic). However, in cases like the interaction between closed-shell molecules in a molecular crystal and the adsorption of closed-shell molecules on metallic surfaces, where we expect a weak chemical interaction, these effects could provide a significant contribution to the total bonding energy. Recent publications addressing this problem show that LDA provides a surprisingly realistic description of the structure (in terms of bonding distances) and energetics of molecular-substrate [48, 49] and molecular crystals [50], when compared with GGA + vdW calculations [48, 51] (vdW effects are added using a semi-empirical scheme [52, 53] to gradient-corrected functionals), and a sophisticated treatment of the correlation energy with the adiabatic connection fluctuation-dissipation theorem (AC-FDT) [49, 50]. LDA certainly has the wrong asymptotic behavior but its well-known tendency to overbind mimics reasonably well the addition of the vdW effects in the relevant distance regime.

In FIREBALL, the valence wave functions are expanded in the FIREBALL orbitals [43, 46], a set of strictly localized pseudoatomic orbitals—they are exactly zero for distances larger than the cutoff radius R_C. We used an optimized basis (see [54] for details) that includes s and p orbitals for C, O, Si and S. The chosen cutoff radii (3.1 and 3.9 a.u. for the s and p S-orbitals, 4.5 a.u. for the s and p C-orbitals, and 4.1 a.u. for the s H-orbital) yield a very good description of the structural and electronic properties of the T6 molecule. The results are in excellent match with fully converged plane-wave DFT calculations (VASP [55–57])—the maximum difference is only 0.02 Å in the bond lengths and 0.5° in the angles—see a detailed comparison in Fig. 1. For the Si oxide cluster that models the apex of our tip, we have used cutoff radius of 3.2 and 3.5 a.u. for the s and p O-orbitals, and 4.8 and 5.4 a.u. for the s and p Si-orbitals.

3.3 Mechanical Characterization of the T6 Molecule and the Monolayer

As a first step, we have carefully characterized the mechanical properties of an isolated T6 molecule and a T6 monolayer in order to understand the deformation patterns observed in our large scale simulations for the tip–sample interaction.

We have explored the mechanical response of both systems under uniform compressing and stretching strains. Starting with the single T6 molecule, and focussing in compression, we can identify three different strength-building mechanisms: changes in the relative orientation of the adjacent thienyl groups (with rotations of these pentagonal rings around the C–C bonds linking these units), bond contraction and folding of the entire molecule. Sub-

unit rotation is by far the cheapest mechanism, as our simulations for the T6 molecule show that the torsional energy around one bond is relatively small—less then 0.1 eV up to 60°.

These three mechanisms are also present in the monolayer case, but the energetics is influenced by the intermolecular interactions associated with the dense packing in the molecular layer. While for the first stages of the deformation process, sub-unit rotation is still an option, the linear (elastic) repulsive response found in the experiments seems to correlate with the competition between folding modes and bond contraction. Given the strength of the carbon–carbon bonds, a deformation based only on bond contraction would lead to large Young's modulus ($\sim$100 GPa), typically associated with solid, crystalline materials. Folding modes reduce that number to tens of GPa, in better agreement with the continuum modelling discussed above.

4 Tip–Sample Force Versus Distance Curves

4.1 Force Calculations with a Quasi-Static Approach at $T = 0$ K

In order to gain insight into the sample deformation mechanisms upon contact with the tip, we have studied the approach and retraction of the Si oxide nanoasperity on five different positions of the unit cell—ranging from top sites on the last atoms to a hollow site between the molecules—and different tip orientations.

The tip–surface interaction has been determined in a stepwise, quasi-static manner by approaching/retracting the tip along the normal to the surface by 0.25 Å. At each approach/retraction step the atoms in both the slab (T6 monolayer) and the tip were allowed to relax to their ground-state configuration using both a conjugate gradient minimization and a dynamical quenching methods. The convergence criteria for the relaxation process are the following: changes in the total energy per atom less than 10^{-5} eV and forces on the free atoms less than 0.1 eV/Å. The bottom carbon atom of each T6 molecule, and the topmost layer of the tip model are kept fixed during the structural minimization process in order to mimic the appropriate boundary conditions. The total short-range tip–sample force was calculated as a sum of the final forces acting on the tip atoms which were kept fixed during the relaxation process at each tip–sample distance.

These forces are shown in Fig. 4. The contact (the zero of the indentation) is defined at the onset of the tip–sample interaction in our first-principles calculations, and corresponds to an approximate distance of 3 Å above the top carbon atoms in the T6 monolayer (see Fig. 3b). Although the detailed evolution of force–distance curves varies among the different positions (see Fig. 4a) and the size of the indentations (up to -1, -2, -3 and -4 Å), all of them share two significant features: very small forces on the attractive regime (as expected from this non-reactive tip),

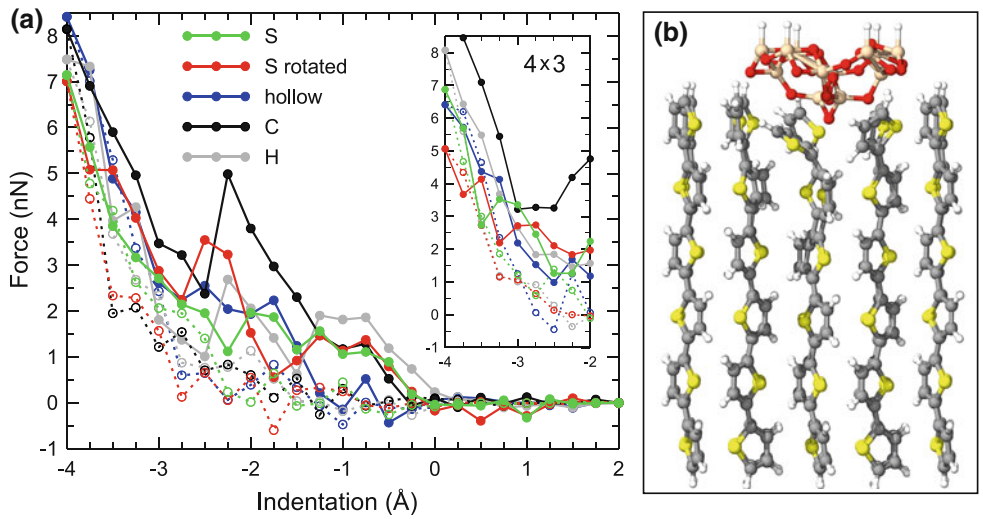

Fig. 4 **a** Force versus distance curves from quasi-static simulations at $T = 0$ K for five different positions of the tip in the 4 × 2 unit cell. The curves show both the approach (*full lines with full circles*) and retraction components (*dashed lines with open circles*). The results for a bigger 4 × 3 unit cell are shown in the *inset*. The zero on the indentation axis is set at the onset of significant tip–sample interaction, and corresponds approximately to a distance of 3 Å between the outermost layer of carbon atoms in the sample and the apex of the tip. **b** Molecular deformation of the T6 monolayer under the tip interaction for an indentations of -4 Å on the S position (some of the molecules in the unit cell have been removed so the deformation in the area directly below the tip can be clearly observed)

and a large hardness in the well defined repulsive 'elastic' regime (forces vary linearly with distance). Figure 4a shows the force versus distance curves for five different positions of the tip (S, S-rotated, hollow, C and H) and the largest indentation considered (−4 Å). The analysis of the stable structures under the nanoasperity shows that the deformation mechanisms are very local, involving significant distortions only in the very few molecules closer to the tip, even for the closest distance (see Fig. 4b). The sample accommodates the load mainly through compression of the bonds along the molecules and rotation of the thiophene subunits closer to the surface.

4.2 Deformation Mechanisms: Competition Between Folding and Stretching Modes

The forces obtained within the previous approach upon indentation of our single nanoasperity are very large compared with both the experiment and the continuum modelling described in the previous sections. This hardness can be an spurious effect associated with two of the limitations of our approach: (1) the size of our simulation cell, and (2) the $T = 0$ K quasi-static approach used in our simulations, where the system can be trapped in some of high-stress local minima.

We have ruled out the influence of our unit cell performing simulations on a larger 4 × 3 unit cell (including now up to 12 T6 molecules and the tip, with 567 atoms in total). Our results for this larger unit cell (see inset in Fig. 4a) confirm the very local character of the induced deformation and the intrinsic mechanical strength on the T6 monolayer. Interestingly, these simulations show a significantly larger contrast in the strong repulsive regime (with differences in the forces between sites up to 3 nN—see the inset in Fig. 4a), that suggest that sub-nanometer resolution could be achieved in the imaging of this system.

The system has a very complicated energy landscape. This is clearly shown by the approach/retraction curves for the larger indentations, where energy barriers which cannot be overcome during the tip retraction cause irreversible deformation of the sample. Although the forces are zero the system is not in a ground state configuration at the end of the approach/retraction cycle as shown by the total energy and confirmed by a direct inspection of the structure of the T6 monolayer. Our study of the mechanical response of both the individual T6 molecule and the T6 monolayer under uniform compression suggests that, in our $T = 0$ K quasi-static approach, the folding modes—where the whole molecule folds in order to accommodate the load (see Fig. 5a)—are frozen and the system is trapped in some high-stress local minima where the mechanical response is dominated by bond compression.

To investigate this issue, we have used a simulated annealing approach, where a short molecular dynamics (MD) simulation (350 fs) at 300 K is used to explore the configurational phase-space is followed by a dynamical quenching method, that brings the system to the ground state. These simulated annealing calculations, starting from some of these high-stress structures have shown that, indeed, there were states with significantly lower repulsive forces (Fig. 5b) that are accessible once the folding modes become active (the barriers between them and the stretching/compressing modes where the system was trapped can be overcome in the presence of temperature).

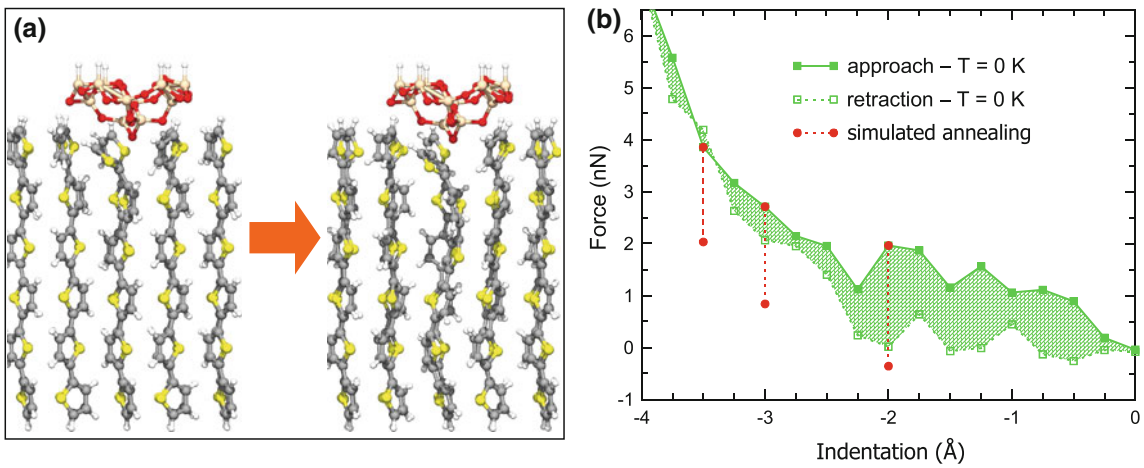

Fig. 5 **a** The structure before (*left*) and after (*right*) the simulated annealing calculation for an indentation of −3.5 Å at the S position. The system relaxes to the true ground state by propagating a deformation along the molecular chain, once the energy barriers that separate the folding modes from the local ground state (characterized by a significant bond compression) can be overcome by the available thermal energy. **b** Forces before and after the simulated annealing for three selected configurations (*red circles*). There is a significant reduction in the repulsive force between tip and sample, compared to the $T = 0$ quasi-static approach (*green lines*), once the folding modes can be accessed. (Color figure online)

4.3 Final Force Calculations Based on Molecular Dynamics Simulations for Each Tip Position

A proper description of the competition between compressing and folding modes is thus crucial for the accurate determination of tip–sample forces under room RT operation. We have faced this problem calculating approach/retraction force curves that include temperature effects, through a collection of MD simulations, on top of different positions in the surface unit cell. For each tip height, we have performed a MD simulation in the canonical ensemble at 300 K. We take the average atomic positions from the previous tip height and displace them vertically by 0.25 Å (approaching/retracting from the sample with the same stepwise procedure considered in the quasi-static simulations), to define the initial configuration for the next MD run. The energy imparted to/taken from the system by moving the tip was removed/added, during some time steps at the beginning of simulation, via the re-scaling of the velocities to keep a constant temperature equal to 300 K. Forces are then calculated for each tip–sample distance during the approach and retraction as a thermal average over all the instantaneous atomic configurations accessed during the corresponding MD simulations. Notice that our MD simulations are not designed to describe how the energy is dissipated along a whole oscillation cycle: they provide an efficient way to include the activated folding modes, that are crucial to describe the mechanical response at RT.

This procedure is very computationally demanding as MD simulations at the ab initio level are extremely time-consuming, even with the fast local-orbital code that we are using (see Sect. 3). Ab initio MD simulations found in the literature are usually limited to 1–2 ps, and here we have to perform an extensive set of MD runs, one for each tip height during approach and retraction on different positions on the the unit cell. In order to show the main qualitative effects brought by temperature, we have applied the methodology described above using short (150 fs) MD simulations with time step of 0.5 fs. Figure 6 shows the force versus distance curves at the S position of the tip obtained from this set of MD simulations for three different indentations: −2, −3 and −4 Å.

These results show how our approach, even with very short MD-simulations, fixes the most important discrepancies between theory and experiment. There is a significant reduction in the forces during the tip approach, due to the activation of the folding modes, and the corresponding dissipated energy per cycle in comparison with our previous $T = 0$ K quasi-static calculations (see the comparison in Fig. 6a). Additionally, the approach/retraction process is now structurally reversible: there is no deformation in the T6 monolayer at the end of the cycle, even for relatively large indentations.

These simulations confirm that the folding modes (see Fig. 5a) are very efficient in reducing the repulsive interaction in the first stages of the indentation process, avoiding the high-stress states where the system was trap in our $T = 0$ K calculations, while the strong repulsive regime (proved by indentations up to −4 Å) was actually well described by the computationally much faster quasi-static approach (see Fig. 6a). These calculations provide a mechanical strength in the first stages of the indentation process in good agreement with the results obtained from

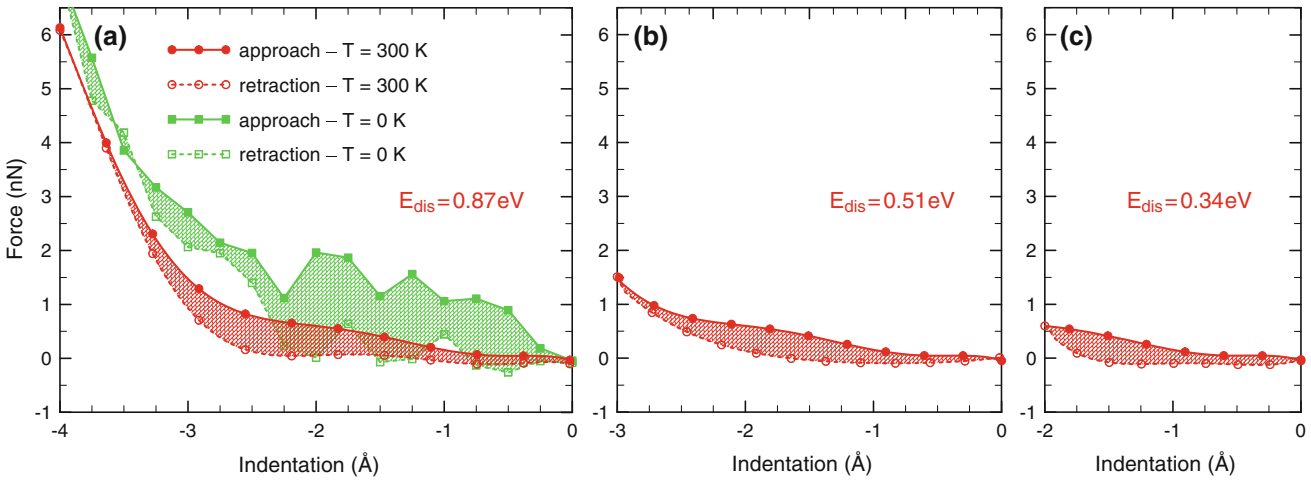

Fig. 6 Force versus distance curves at the S position (tip initially on top of a sulphur atom on the T6 molecule) for three different indentations: **a** −4 Å, **b** −3 Å and **c** −2 Å. The *red curves* show the normal force during approach (*full lines with full circles*) and retraction (*dashed lines with open circles*) calculated from individual short (150 fs) MD runs at $T = 300$ K for each tip height. The energy dissipated per cycle (equal to the area enclosed by the hysteresis curve) is indicated. Results for quasi-static calculations at $T = 0$ K (*green curves*) are shown for comparison. (Color figure online)

the continuum modelling of the experimental force curves. They also bring the energy dissipation values within the order of magnitude of the experimental results and illustrate their dependence with the indentation depth.

However, those simulations are still not long enough to provide accurate values for the force hysteresis and thus for the dissipated energy. We have then applied the same methodology to long (2 ps) MD simulations with time step of 0.5 fs. Given the computational demands, we have restricted ourselves to two positions on the surface unit cell—position S (tip initially on top of a sulphur atom) and the hollow position (between the molecules)—and to the soft indentation regime (up to −2 Å) proved in the experiments shown in Fig. 2. Figure 7a shows the approach/retraction force curves calculated in this way. Besides those force curves, we also show the instantaneous values (insets in Fig. 7a) and the average for each force component (b and c panels in Fig. 7) for the first 1.5 ps for two of these simulations. They correspond to approach and retraction for position S and zero indentation (the blue circles in Fig. 7a). The average at a given time is calculated with all the previous configurations, discarding the ones corresponding to the first 0.5 ps of evolution. Notice that the average force values are already converged after 1.5 ps. This is also the case for simulations close to the maximum indentation—see Fig. 8. Tests performed with 5 ps simulations on certain tip positions and the study of the time evolution of the force components show that the average force values are converged to an accuracy of 0.02 nN.

The average normal force in Fig. 8 reveals the force hysteresis between the tip approach and retraction—those positions correspond to the blue squares in Fig. 7a. The importance of the temperature and the proper sampling of the configurational phase-space in determining those values is revealed by the clear difference between the insets in Fig. 7a and the lower panels in Fig. 8. In the strong interaction regime, the large, circular shape of the F_x versus F_y plot for the whole MD simulation confirms that the system is indeed able to visit the whole configurational phase-space accessible at 300 K.

Our first principles simulations provide a quantitative determination of the energy dissipation associated with the short-range force hysteresis. The observable force versus distance values do depend on history (loading vs. unloading). While the details of the force curves on top of the two different sites are clearly different—in the hollow position, most of the energy is dissipated during the first half of the indentation, while on an S position the hysteresis occurs at the end of the indentation—the total dissipated energy is very similar (0.14 vs. 0.16 eV).

In Sect. 2, we have shown that the energy dissipated in the experiments exclusively through short-range forces for the same indentation of −2 Å is 1.4 eV/cycle. This short-range contribution to the total energy dissipation—taken place during the mechanical contact—was determined from dynamic dissipation curves taken in both attractive and repulsive regimes with the aid of contact mechanics modelling. To make a quantitative comparison between the experiment and first-principles calculations for a single nanoasperity, we notice that the experimental contact area ($\sim$3.1 nm^2) estimated for a −2.0 Å indentation, is large compared with an individual molecular contact

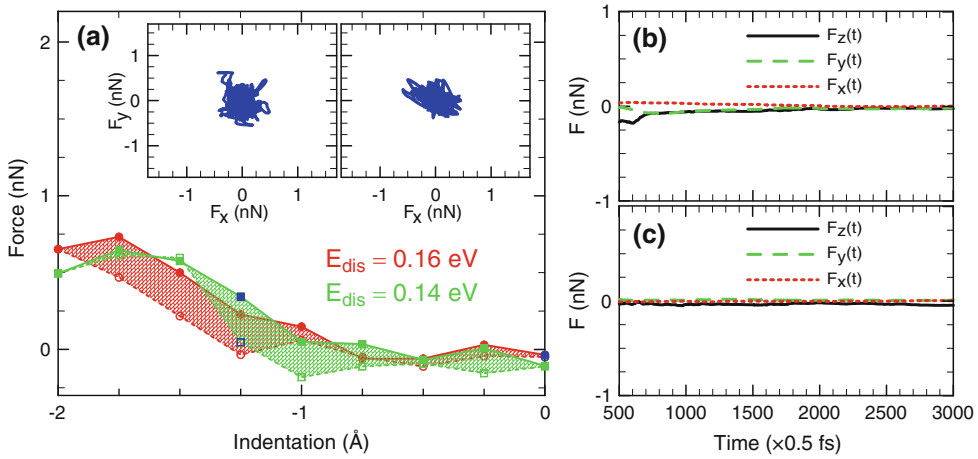

Fig. 7 **a** Force–distance curves at a hollow position between molecules (*green, squares*) and over a sulphur atom (*red, circles*) calculated from individual 2 ps long MD runs at $T = 300$ K for each tip height. The normal forces during approach (*continuous lines with full symbols*) and retraction (*dashed lines with open symbols*) are calculated as an average over all the instantaneous configurations, discarding the ones corresponding to the first 0.5 ps. **b** and **c** displayed the average of the x, y, z-force components as a function of the simulation time for two of those MD simulations, corresponding to the same tip position (over the sulphur atom) and height (zero indentation) for approach **b** and retraction **c**. The *insets* in **a** show F_x versus F_y for each time step for the same two MD simulations. (Color figure online)

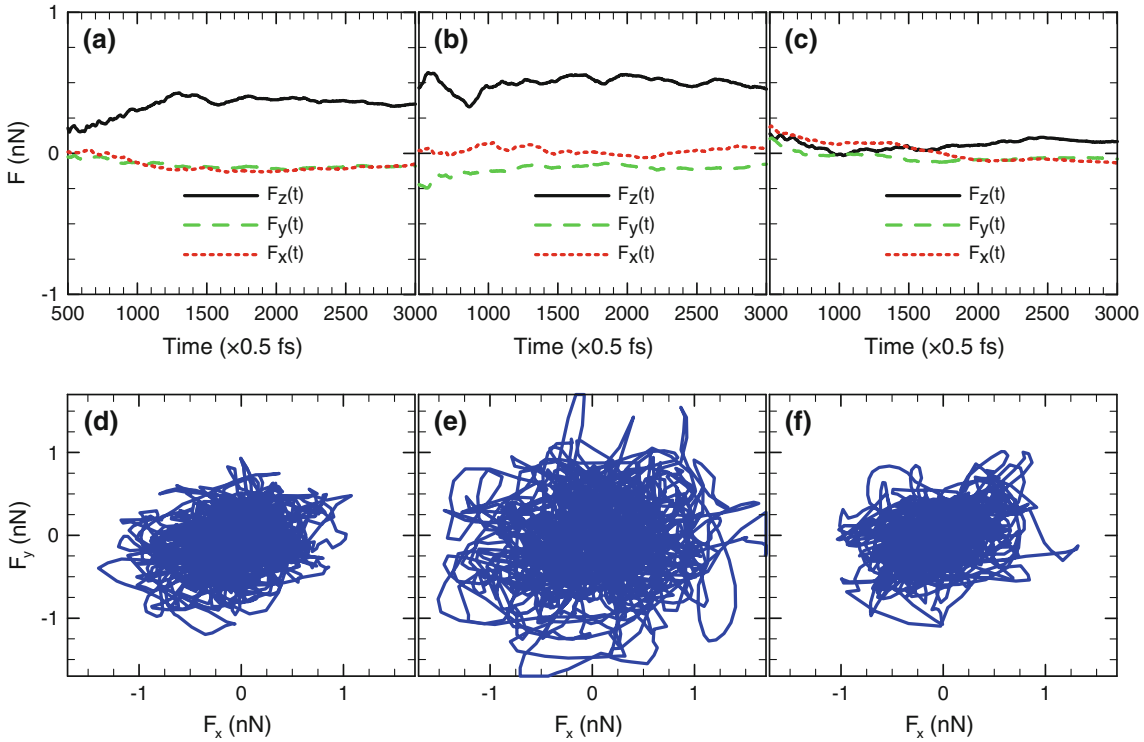

Fig. 8 *Top panels*: time evolution of the average of the *x*, *y*, *z*-force components for three 2 ps MD simulations corresponding to the same tip position (hollow) and different tip heights: for an indentation of −1.25 Å in the approach **a** and retraction **c**, and for the minimum tip–sample distance **b**—an indentation of −2 Å. *Lower panels* **d**–**f**: F_x versus F_y for each time step in the same three MD simulations as in *top panels*

(∼0.4 nm^2) used for a single nano-asperity. As we have shown that deformation mechanisms are very local and that the dissipated energy is very similar for the different tip positions, we can simply scale up the nano-asperity area ∼0.4 nm^2 to the experimental contact area ∼3.1 nm^2. Then, the experimental value ∼1.4 eV is in good agreement with the one deduced from first-principles simulations (1.2 = 8 × 0.15 eV) by involving eight individual molecular contacts.

5 Adhesion Hysteresis as the Relevant Dissipation Mechanism

Several mechanisms have been proposed to explain the lost of mechanical energy in dynamical AFM including viscous damping associated to the displacement of charge carriers [24], stochastic [58, 59] and vdW [60] friction, capillary forces [39], and adhesion hysteresis [29, 31, 32, 35, 61]. Their strength can be significantly affected by the relative velocity [13, 24], temperature [35], tip and sample mechanical properties [21], and tip–sample distance regime (e.g. non-contact vs. indentation [61]). Some of them, like those mediated by electrical or magnetic interactions, are responsible for the long-range contribution to dissipation. Here, we focus on the two mechanisms, stochastic friction [58, 59] and adhesion hysteresis [29, 31, 32, 35, 61] that are widely suggested to be responsible for the observed dissipation in dynamic AFM in the near-contact regime. In the stochastic friction force mechanism, the energy dissipation is attributed to the coupling of the fluctuations around the equilibrium atomic positions in the tip and sample through their mutual interaction. This nonequilibrium phenomenon results in the friction force proportional to the tip velocity with the coefficient given by the time integral of the time correlation function of the fluctuating tip–surface force. As dissipation images have nanometer- or, even atomic-scale resolution (in the case of the FM-AFM), the interaction responsible for the coupling must be essentially short-range and decay rapidly with the distance. Due to this short-range character, numerical estimates of the energy dissipation associated to this mechanism lead to severely underestimated results.

According to the adhesion hysteresis mechanism, forces during approach and retraction are different due to non-adiabatic relaxation of the surface atoms when the tip comes very close to the surface, leading to the lost of the characteristic energy associated with these atomistic processes in every oscillation cycle. Our first-principles simulations support this mechanism, provide a quantitative

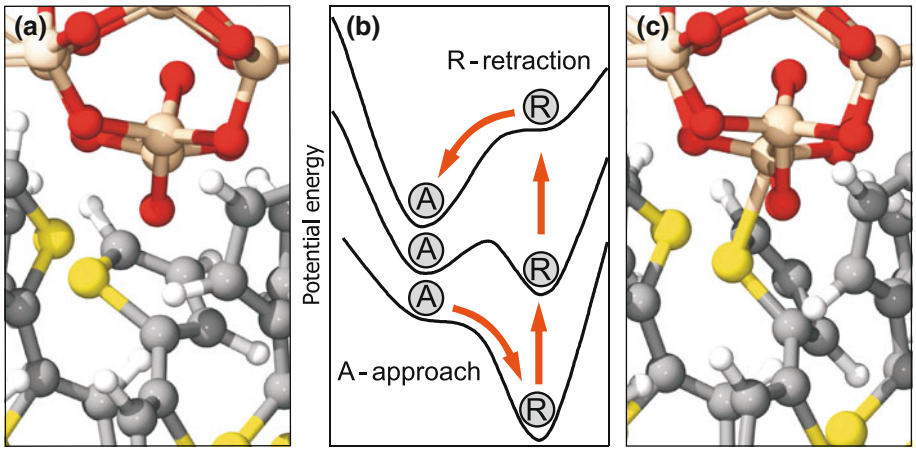

Fig. 9 Thermal-averaged configurations (calculated as an average of the individual atomic coordinates along the corresponding 2 ps MD simulations performed in the canonical ensemble at 300 K) for the same tip position (over the sulphur atom) and tip height (an indentation of −1.5 Å) for approach **a** and retraction **c**. Notice that the bonds formed during further indentation from this tip–sample distance control the adhesive response in the retraction stage. The configuration space sampled by the tip depends on whether the tip approaches (configuration A) or withdraws (configuration R: the S–Si bond is formed) from the surface. **b** A schematic illustration of how the potential energy surface changes due to tip influence during this structurally reversible cycle

determination of the energy dissipation at the atomic scale and give insight into the molecular mechanisms associated with the short-range force hysteresis. The hysteretic behaviour can be understood in terms of the complicated energy landscape of metastable molecular configurations that the system can adopt for a given tip position. This is obviously complicated when temperature is present and the system can explore the configurational phase-space. However, thermal-averaged configurations (calculated as an average of the individual atomic coordinates along the MD run, in the same way as the averaged forces discussed above) can help to illustrate the fact that the system stays close to different local energy minima during the approach and retraction stages. Figure 9a, c shows the averaged atomic coordinates of the system (for 2 ps MD simulations) during approach and retraction for the same indentation of −1.5 Å. Notice that the bonds formed during further indentation from this tip–sample distance control the adhesive response in the retraction stage. The system is trapped, due to the presence of energy barriers that cannot be overcome even with the available thermal energy, in different bonding configurations corresponding to local energy minima during the approach and retraction of the tip. These energy barriers are responsible for breaking the adiabaticity and thus lead to energy dissipation (this is schematically illustrated in Fig. 9b).

Thus, these simulations provide a quantitative confirmation—on a complex, real material—of the mechanism proposed by Sasaki and Tsukada [62], further elaborated, by Kantorovich and Trevethan [29], and revealed by our previous combined experimental–theoretical study with the FM-AFM of the ultimate case of a single adhesive bond [31]: the force hysteresis is originated by the existence of two or more solutions in the force upon approaching and retracting the tip over the surface, and this hysteresis leads to the observed energy dissipation. The forces during approach and retraction are different due to distinct states occupied by the system at different stages in the tip trajectory. The work done by the tip will be equal to the area enclosed by the hysteresis curve and this energy will be dissipated into local phonons as the system moves from one state into the other.

The adhesion hysteresis shown above is compatible with structurally reversible processes, despite the fact that those processes are strictly statistically irreversible. It states that for a given tip–surface distance there is a unique total energy surface. This surface has several local minima with respect to the atomic positions. The hysteresis appears because the observable atomic positions do depend on the history of the tip motion. Essentially, the mechanism is very similar, considering a tip displacements normal to the surface, to the Tomlinson model frequently invoked to introduce atomic-scale friction during lateral tip motion [22].

6 Conclusions

Our extensive ab initio theoretical study shows the nature of molecular energy-dissipation processes at room temperature in sexithiophene monolayers. Those processes involve different equilibrium positions for the atoms interacting with the tip during the loading and unloading cycles, resulting in force hysteresis. The system is trapped, due to the presence of energy barriers that cannot be overcome even with the available thermal energy, in

different bonding configurations corresponding to local energy minima during the approach and retraction of the tip. These energy barriers are responsible for breaking the adiabaticity and thus lead to energy dissipation. Our study highlights the importance of including the folding modes of the T6 molecules, frozen at $T = 0$ K, in order to describe properly the mechanical response of the system. We have devised an approach, based on performing long (2 ps) MD simulations at $T = 300$ K for each tip height, that brings the theoretical short-range forces to a good agreement with the experiment and allows a quantitative comparison of the dissipated energy.

Our work shows that the phase-signal contrast arising in AM-AFM can be explained with non-invasive, reversible atomic and molecular reorganization processes. Furthermore, the quantitative agreement between first-principles calculations, dynamic simulations based in continuum modelling, and experiment supports the use of AM-AFM as a tool to investigate dissipation processes and the role of adhesion hysteresis as a dominant mechanism for energy dissipation. This idea can be extended to other dynamic operation modes for the AFM, in particular those like the FM-AFM that can achieve atomic resolution. A combination of force spectroscopy experiments with first-principles simulations have identified a dissipation channel associated with the properties of a single atomic contact and provide a detailed atomistic description of the process [31, 32]. Understanding how the energy-dissipation processes associated with friction are quantitatively affected by the contact geometry, adhesion forces, contaminants and atomic-scale defects is the next challenge. Recent extensions of the FM-AFM technique to map the three dimensional surface force field with picometer and piconewton resolution [63, 64] promise to open a new avenue for the characterization and understanding of friction at the atomic scale.

Acknowledgments This work has been financially supported by the European Commission (FORCETOOL, NMP4-CT-2004-013684), the Spanish Ministry of Science and Innovation (MICINN) under projects MAT2008-02929-NAN and the ESF EUROCORES FANAS Programme (AFRI Project, MAT2008-02939-E). Computer time provided by the Spanish Supercomputing Network (RES) at the Tirant Supercomputer and by the Centro de Supercomputación y Visualización de Madrid (CeSViMa) is gratefully acknowledged.

References

1. Urbakh, M., Klafter, J., Gourdon, D., Israelachvili, J.: The nonlinear nature of friction. Nature **430**, 525–528 (2004)
2. Persson, B.N.J.: Sliding Friction: Physical Principles and Applications, 2nd edition. Springer-Verlag, Berlin (2000)
3. García, R., Pérez, R.: Dynamic atomic force microscopy methods. Surf. Sci. Rep. **47**, 197–301 (2002)
4. Stroh, C., Wang, H., Bash, R., Ashcroft, B., Nelson, J., Gruber, H., Lohr, D., Lindsay, S.M., Hinterdorfer, P.: Single-molecule recognition imaging microscopy. Proc. Natl Acad. Sci. USA **101**, 12503–12507 (2004)
5. Yokokawa, M., Wada, C., Ando, T., Sakai, N., Yagi, A., Yoshimura, S.H., Takeyasu, K.: Fast-scanning atomic force microscopy reveals the ATP/ADP-dependent conformational changes of GroEL. EMBO J. **25**, 4567–4576 (2006)
6. Pérez, R., Payne, M., Štich, I., Terakura, K.: Role of covalent tip-surface interactions in noncontact atomic force microscopy. Phys. Rev. Lett. **78**, 678–681 (1997)
7. Livshits, A.I., Shluger, A.L., Rohl, A.L., Foster, A.S.: Model of noncontact scanning force microscopy on ionic surfaces. Phys. Rev. B **59**, 2436–2448 (1999)
8. Lantz, M.A., Hug, H.J., Hoffmann, R., van Schendel, P. J.A., Kappenberger, P., Martin, S., Baratoff, A., Güntherodt, H.-J.: Quantitative measurement of short-range chemical bonding forces. Science **291**, 2580–2583 (2001)
9. Hoffmann, R., Kantorovich, L.N., Baratoff, A., Hug, H.J., Güntherodt, H.-J.: Sublattice identification in scanning force microscopy on alkali halide surfaces. Phys. Rev. Lett. **92**, 146103 (2004)
10. Fukuma, T., Ichii, T., Kobayashi, K., Yamada, H., Matsushige, K.: True-molecular resolution imaging by frequency modulation atomic force microscopy in various environments. Appl. Phys. Lett. **87**, 034101 (2005)
11. Fukuma, T., Higgins, M.J., Jarvis, S.P.: Direct imaging of lipid-ion network formation under physiological conditions by frequency modulation atomic force microscopy. Phys. Rev. Lett. **98**, 106101 (2007)
12. García, R., Magerle, R., Pérez, R.: Nanoscale compositional mapping with gentle forces. Nat. Mater. **6**, 405–411 (2007)
13. Tamayo, J., García, R.: Relationship between phase shift and energy dissipation in tapping-mode scanning force microscopy. Appl. Phys. Lett. **73**, 2926–2928 (1998)
14. Anczykowski, B., Gotsmann, B., Fuchs, H., Cleveland, J.P., Elings, V.B.: How to measure energy dissipation in dynamic mode atomic force microscopy. Appl. Surf. Sci. **140**, 376–382 (1999)
15. Martin, P., Marsaudon, S., Aimé, J.P., Bennetau, B.: Experimental determination of conservative and dissipative parts in the tapping mode on a grafted layer: comparison with frequency modulation data. Nanotechnology **16**, 901–907 (2005)
16. Johnson, K.L., Kendall, K., Roberts, A.D.: Surface energy and the contact of elastic solids. Proc. R. Soc. Lond. **A324**, 301–313 (1971)
17. Derjaguin, B.V., Muller, V.M., Toporov, Y.P.: Effect of contact deformations an adhesion of particles. J. Colloid Interface Sci. **53**, 314–326 (1975)
18. Paulo, A.S., García, R.: Unifying theory of tapping-mode atomic-force microscopy. Phys. Rev. B **66**, 041406–041409 (2002)
19. Lee, M., Jhe, W.: General theory of amplitude-modulation atomic force microscopy. Phys. Rev. Lett. **97**, 036104 (2006)
20. Hölscher, H., Schwarz, U.D.: Theory of amplitude modulation atomic force microscopy with and without q-control. Int. J. Non-Linear Mech. **42**, 608 (2007)
21. García, R., Gómez, C., Martínez, N.F., Patil, S., Dietz, C., Magerle, R.: Identification of nanoscale dissipation processes by dynamic atomic force microscopy. Phys. Rev. Lett. **97**, 016103 (2006)
22. Giessibl, F.J., Herz, M., Mannhart, J.: Friction traced to the single atom. Proc. Natl Acad. Sci. USA **99**, 12006–12010 (2002)
23. Morita, S., Wiesendanger, R., Meyer, E.: Noncontact Atomic Force Microscopy. NanoScience and Technology. Springer-Verlag, Berlin (2002)
24. Denk, W., Pohl, D.W.: Local electrical dissipation imaged by scanning force microscopy. Appl. Phys. Lett. **59**, 2171–2173 (1991)

25. Loppacher, C., Bennewitz, R., Pfeiffer, O., Guggisberg, M., Bammerlin, M., Schär, S., Barwich, V., Baratoff, A., Meyer, E.: Experimental aspects of dissipation force microscopy. Phys. Rev. B **62**, 13674–13679 (2000)
26. Bennewitz, R., Foster, A.S., Kantorovich, L.N., Bammerlin, M., Loppacher, C., Schär, S., Guggisberg, M., Meyer, E., Shluger, A.L.: Atomically resolved edges and kinks of NaCl islands on Cu(111): experiment and theory. Phys. Rev. B **62**, 2074–2084 (2000)
27. Hug, H.J., Baratoff, A.: Noncontact Atomic Force Microscopy, Chap. 20, pp. 395–432. Springer-Verlag, New York (2002)
28. Gauthier, M., Pérez, R., T.Arai, M.T., Tsukada, M.: Interplay between nonlinearity, scan speed, damping, and electronics in frequency modulation atomic-force microscopy. Phys. Rev. Lett. **89**, 146104 (2002)
29. Kantorovich, L.N., Trevethan, T.: General theory of microscopic dynamical response in surface probe microscopy: from imaging to dissipation. Phys. Rev. Lett. **93**, 236102 (2004)
30. Cross, G., Schirmeisen, A., Stalder, A., Grütter, P., Tschudy, M., Durig, U.: Adhesion interaction between atomically defined tip and sample. Phys. Rev. Lett. **80**, 4685–4688 (1998)
31. Oyabu, N., Pou, P., Sugimoto, Y., Jelínek, P., Abe, M., Morita, S., Pérez, R., Custance, O.: Single atomic contact adhesion and dissipation in dynamic force microscopy. Phys. Rev. Lett. **96**, 106101 (2006)
32. Sugimoto, Y., Pou, P., Custance, O., Jelínek, P., Abe, M., Pérez, R., Morita, S.: Complex patterning by vertical interchange atom manipulation using atomic force microscopy. Science **322**, 413–417 (2008)
33. Porzio, W., Destri, S., Mascherpa, M., Brüeckner, S.: Structural aspects of oligothienyl series from x-ray powder diffraction data. Acta. Polym. **44**, 266–272 (1993)
34. Horowitz, G., Bachet, B., Yassar, A., Lang, P., Demanze, F., Fave, J.L., Garnier, F.: Growth and characterization of sexithiophene single crystals. Chem. Mater. **7**, 1337–1341 (1995)
35. Martínez, N.F., Kamiński, W., Gómez, C.J., Albonetti, C., Biscarini, F., Pérez, R., and García, R.: Molecular scale energy dissipation in oligothiophene monolayers measured by dynamic force microscopy. Nanotechnology **20**, 434021 (2009)
36. Martínez, N.F., García, R.: Measuring phase shifts and energy dissipation with amplitude modulation atomic force microscopy. Nanotechnology **17**, S167–S172 (2006)
37. Hu, S., Raman, A.: Chaos in atomic force microscopy. Phys. Rev. Lett. **96**, 036107 (2006)
38. Rodríguez, T.R., García, R.: Tip motion in amplitude modulation tapping-mode atomic-force microscopy: Comparison between continuous and point-mass models. Appl. Phys. Lett. **80**, 1646 (2002)
39. Yoshizawa, H., Chen, Y.L., Israelachvili, J.: Fundamental mechanisms of interfacial friction. 1. Relation between adhesion and friction. J. Phys. Chem. **97**, 4128 (1993)
40. Moulin, J.F., Dinelli, F., Massi, M., Albonetti, C., Kshirsagar, R., Biscarini, F.: In situ x-ray synchrotron study of organic semiconductor ultrathin films growth. Nucl. Instrum. Methods Phys. Res. B **246**, 122–126 (2006)
41. Bromley, S.T., Zwijnenburg, M.A., Maschmeyer, T.: Fully coordinated silica nanoclusters: $(SiO_2)_n$ molecular rings. Phys. Rev. Lett. **90**, 035502 (2003)
42. Zwijnenburg, M.A., Bromley, S.T., Flikkema, E., Maschmeyer, T.: Prospects for a synthetic route towards well-defined stoichiometric silica nanoclusters: from siloxane to silica. Chem. Phys. Lett. **385**, 389 (2004)
43. Sankey, O.F., Niklewski, D.J.: Ab initio multicenter tight-binding model for molecular-dynamics simulations and other applications in covalent systems. Phys. Rev. B **40**, 3979–3995 (1989)
44. Demkov, A.A., Ortega, J., Sankey, O.F., Grumbach, M.P.: Electronic structure approach for complex silicas. Phys. Rev. B **52**, 1618–1630 (1995)
45. Lewis, J.P., Glaesemann, K.R., Voth, G.A., Fritsch, J., Demkov, A.A., Ortega, J., Sankey, O.F.: Further developments in the local-orbital density-functional-theory tight-binding method. Phys. Rev. B **64**, 195103 (2001)
46. Jelínek, P., Wang, H., Lewis, J.P., Sankey, O.F., Ortega, J.: Multicenter approach to the exchange-correlation interactions in ab initio tight-binding methods. Phys. Rev. B **71**, 235101–235109 (2005)
47. Kohn, W., Sham, L.J.: Self-consistent equations including exchange and correlation effects. Phys. Rev. **140**, A1133–A1138 (1965)
48. Rohlfing, M., Temirov, R., Tautz, F.S.: Adsorption structure and scanning tunneling data of a prototype organic-inorganic interface: PTCDA on Ag(111). Phys. Rev. B **76**, 115421 (2007)
49. Rohlfing, M., Bredow, T.: Binding energy of adsorbates on a noble-metal surface: exchange and correlation effects. Phys. Rev. Lett. **101**, 266106 (2008)
50. Lu, D., Li, Y., Rocca, D., Galli, G.: Ab initio calculation of van der Waals bonded molecular crystals. Phys. Rev. Lett. **102**, 206411 (2009)
51. Romaner, L., Nabok, D., Puschnig, P., Zojer, E., Ambrosch-Draxl, C.: Theoretical study of PTCDA adsorbed on the coinage metal surfaces, Ag(111), Au(111) and Cu(111). New J. Phys. **11**, 053010 (2009)
52. Grimme, S.: Accurate description of van der Waals complexes by density functional theory including empirical corrections. J. Comput. Chem. **25**, 1463–1473 (2004)
53. Elstner, M., Hobza, P., Frauenheim, T., Suhai, S., Kaxiras, E.: Hydrogen bonding and stacking interactions of nucleic acid base pairs: a density-functional-theory based treatment. J. Chem. Phys. **114**, 5149–5155 (2001)
54. Basanta, M.A., Dappe, Y.J., Jelínek, P., Ortega, J.: Optimized atomic-like orbitals for first-principles tight-binding molecular dynamics. Comput. Mater. Sci. **39**, 759–766 (2007)
55. Kresse, G., Hafner, J.: Ab initio molecular dynamics for liquid metals. Phys. Rev. B **47**, R558 (1993)
56. Kresse, G., Furthmüller, J.: Efficiency of ab-initio total energy calculations for metals and semiconductors using a plane-wave basis set. Comput. Mater. Sci. **6**, 15 (1996)
57. Kresse, G., Furthmüller, J.: Efficient iterative schemes for ab initio total-energy calculations using a plane-wave basis set. Phys. Rev. B **54**, 11169 (1996)
58. Gauthier, M., Tsukada, M.: Theory of noncontact dissipation force microscopy. Phys. Rev. B **60**, 11716 (1999)
59. Kantorovich, L.N.: Stochastic friction force mechanism of energy dissipation in noncontact atomic force microscopy. Phys. Rev. B **64**, 245409 (2001)
60. Volokitin, A.I., Persson, B.N.J.: Resonant photon tunneling enhancement of the van der Waals friction. Phys. Rev. Lett. **91**, 106101 (2003)
61. Schirmeisen, A., Hölscher, H.: Velocity dependence of energy dissipation in dynamic force microscopy: hysteresis versus viscous damping. Phys. Rev. B **72**, 045431 (2005)
62. Sasaki, N., Tsukada, M.: Effect of microscopic nonconservative process on noncontact atomic force microscopy. Jpn. J. Appl. Phys. **39**, L1334 (2000)
63. Albers, B.J., Schwendemann, T.C., Baykara, M.Z., Pilet, N., M.Liebmann, E.I.A., Schwarz, U.D.: Three-dimensional imaging of short-range chemical forces with picometre resolution. Nat. Nanotechnol. **4**, 307–310 (2009)
64. Gross, L., Mohn, F., Moll, N., Liljeroth, P., Meyer, G.: The chemical structure of a molecule resolved by atomic force microscopy. Science **325**, 1110–1114 (2009)